

Article

Coupling Study on Quasi-Static and Mixed Thermal Elastohydrodynamic Lubrication Behavior of Precision High-Speed Machine Spindle Bearing with Spinning

Hao Liu ^{1,2}, Yun Chen ^{1,*}, Yi Guo ¹, Yongpeng Shi ¹, Dianzhong Li ¹ and Xing-Qiu Chen ^{1,*}

¹ Shenyang National Laboratory for Materials Science, Institute of Metal Research, Chinese Academy of Sciences, Shenyang 110016, China; hliu20b@imr.ac.cn (H.L.)

² School of Materials Science and Engineering, University of Science and Technology of China, Hefei 230026, China

* Correspondence: chenyun@imr.ac.cn (Y.C.); xingqiu.chen@imr.ac.cn (X.-Q.C.)

Abstract: In this work, a modified numerical algorithm that couples the quasi-static theory with the mixed thermal elastohydrodynamic lubrication (mixed-TEHL) model is proposed to examine the mechanical properties and lubrication performance of the spindle bearing that is used in a high-speed machine tool with spinning. The non-Newtonian fluid characteristics of the lubricant and the non-Gaussian surface roughness are also considered. Moreover, the mechanical properties and lubrication state of the bearing are examined in various service environments. The results indicate that the temperature reduces the lubrication efficiency, which in turn exerts a significant impact on the mechanical properties. The lubrication that either behaves in the manner of Newtonian or non-Newtonian fluid has a relatively negligible influence on the bearing working state, while the non-Gaussian surface roughness significantly alters the oil film thickness and temperature. Calculations with different operating conditions demonstrate that the operating parameters (i.e., axial load, rotation speed) will directly affect the performance of the bearings via the changes in the oil film thickness and the temperature.

Keywords: angular contact ball bearing; mixed thermal elastohydrodynamic lubrication; mechanical characteristics; lubrication state



Citation: Liu, H.; Chen, Y.; Guo, Y.; Shi, Y.; Li, D.; Chen, X.-Q. Coupling Study on Quasi-Static and Mixed Thermal Elastohydrodynamic Lubrication Behavior of Precision High-Speed Machine Spindle Bearing with Spinning. *Machines* **2024**, *12*, 325. <https://doi.org/10.3390/machines12050325>

Academic Editors: Dongwu Li and Yaguang Wu

Received: 8 April 2024

Revised: 1 May 2024

Accepted: 2 May 2024

Published: 9 May 2024



Copyright: © 2024 by the authors. Licensee MDPI, Basel, Switzerland. This article is an open access article distributed under the terms and conditions of the Creative Commons Attribution (CC BY) license (<https://creativecommons.org/licenses/by/4.0/>).

1. Introduction

The spindle bearing is a key component that determines the service performance of a machine tool. For a long time, the industry has generally accepted that fatigue and fracture are the primary causes of spindle bearing failure. However, with the updating of the bearing material design and processing technologies, failures related to the reliability of dimensional precision are becoming increasingly prominent, in particular for bearings in high-precision machine tools under high-speed rotation [1]. In more cases, the complex spinning–sliding–rolling motion within the micro-contact region of the bearing induces friction spalling of the surface materials and thus leads to the bearing’s original working precision being lost [2]. Additionally, this mixed motion increases the temperature of the lubricant [3,4], weakens the lubrication performance [5], and further aggravates the wear failure.

To date, abundant research on thermal elastohydrodynamic lubrication (TEHL) with spinning has been conducted. Doki-Thonon et al. [6] successfully developed a TEHL model for non-Newtonian fluids with spinning. They found that the spinning not only caused the lubricating oil film to exhibit asymmetry but also caused a thermal thinning effect, resulting in a 60% and 40% reduction in the minimum oil film thickness and central oil film thickness, respectively. Pu et al. [7] proposed an approach to tackle elliptical contact in mixed lubrication under the influence of any velocity vector. Recently, Yan et al. [8,9]

studied the effect of spinning on mixed TEHL and fatigue life with the introduction of sinusoidal surface roughness. In terms of experiments, Doki-Thonon et al. [10] analyzed the influence of spinning on the TEHL oil film thickness using the tribology experimental platform, and a mixture of Squalene and 15 wt.% of Polyisoprene was selected as the lubricant. The in situ measurement results were in excellent agreement with the numerical analysis results of Ref. [6]. Amine et al. [11] investigated oil film thickness and friction in the TEHL under the sliding condition, from pure rolling to opposite sliding, on the barrel-on-disk tribometer. The friction coefficient measured experimentally increased with the slide-to-roll ratio (SRR) and tended to be stable at a high SRR. Nevertheless, the objective of the aforementioned research is to solve the EHL problem under the assumption that the mechanical properties and motion states are predetermined. However, the EHL analysis cannot accurately reflect the effect of ball bearing structural parameters and operating conditions on the EHL performance. Bearing mechanical property analysis is essentially related to bearing lifetime and lubrication performance. Moreover, the contact forces will be distinct from those obtained by applying the Hertzian theory and EHL on the same contact [12]. Neglecting the oil film and employing the Hertzian approach will lead to a misestimation of contact force in the lubricated bearings [13]. Therefore, an effective coupling algorithm is necessary in order to predict the potential issues, such as inadequate lubrication and wear failure. Currently, due to its reliable accuracy, resilient application, and exceptional operating efficiency, the quasi-static model based on the “outer raceway control theory” developed by Jones et al. [14] is still the most preferred model used in the study of bearing mechanical properties.

Concerning the coupling analysis of bearing mechanical properties with EHL, Shi et al. [15] have developed a coupling numerical algorithm by integrating the quasi-dynamic model with TEHL equations, which was then used to evaluate the lubrication state of high-speed and heavy-load angular contact ball bearings with spinning, and the aero lubricant 4109 was selected as the lubricant. Li et al. [16] have established a model of mixed lubrication based on the moving point heat source integral method by combining the quasi-static model of high-speed angular contact bearings with the non-Newtonian TEHL. Bal et al. [17] examined EHL within the quasi-static model of angular contact ball bearings. In their work, the Hamrock–Dowson (H&D) [18] empirical formula of film thickness was used to calculate the central film thickness, and the central film thickness was then superimposed on the dry contact elastic deformation to determine the displacement of a rigid body under lubrication. However, Sun et al. [19] argued that the numerical solution of film thickness at high-speed and heavy load was two to four times that of the empirical H&D formula. Guo et al. [20] adapted the empirical formula of the rigid body central film thickness with spinning and incorporated it into the quasi-static model. However, the range of the fitting conditions was constrained, and the error of the empirical formula for minimum film thickness at high-speed exceeded 20%. Tian et al. [21] coupled the bearing dynamic model with the TEHL and computed the contact force, temperature, and film thickness in the contact area, taking spinning and non-Newtonian effects into consideration. Wu et al. [22] employed mixed EHL coupled with a quasi-dynamic model to investigate the angular contact bearings under low-speed and heavy-load conditions. To address the damage problems introduced by skidding behavior, Gao et al. [23] proposed a kinematic Hertzian contact TEHL model, which considered the dynamic characteristics of bearings and quasi-static analysis on load distribution and deformation of the bearing parts, in which the lubricant type was SAE20W40. Shuai et al. [24] established the mechanical analysis model of angular contact bearings and analyzed the effect of various preloading modes on bearing contact load and oil film thickness. Furthermore, the lubrication performance of the contact pair is significantly affected by the surface texture. Hence, Peta et al. [25] chose Ti6Al4V, a commonly used material in biomedicine, as the research object. They aimed to enhance the lubrication performance between the bones and the biomaterials by altering the surface texture properties of titanium alloys. However, it is noted that this research did not encompass bearing applications. Zmarzly [26] examined the influence of the surface

topography of bearing raceways on the vibration values of the bearing system, and a concept of operational heredity was presented. The experimental results showed that the surface texture directly affects the vibration values of the bearing, which in turn allows for the assessment of the bearing's operational stability. However, this study failed to include an investigation of the mechanical states and lubrication performance of the bearing.

In terms of the above research, several unresolved issues remain outstanding in the coupling analysis of the mechanical properties and the EHL of ball bearings. Firstly, many studies still rely on fitting the empirical formula to calculate the film thickness. However, the empirical formula is limited to specific operating conditions and is incapable of coupling in spinning, temperature, or contact morphology. Secondly, existing models mostly employ Hertzian contact stiffness to calculate the contact load of the mechanical model without considering the effect of oil film stiffness, resulting in reduced accuracy in the examination of mechanical properties in the ball-ring micro-contact zone. Thirdly, current investigations demonstrate that the surface topography of the contact pair impacts the lubrication performance of the micro-contact zone, which is well accepted in biomedicine. However, this is generally neglected in bearing applications. Consequently, incorporating the EHL into the bearing mechanics model requires further investigation with more critical factors taken into consideration. Therefore, in this paper, a study on the coupling of the quasi-static model and mixed TEHL is conducted, using a 7008C high-speed and high-precision machine spindle bearing as the research object. To comprehensively examine the coupling between mechanical properties and lubrication states, this paper is organized as follows:

- (1) This work develops a mixed lubrication model that encompasses boundary lubrication to full-film lubrication, expanding the calculation application to the presence of non-full-film lubrication in actual operating conditions.
- (2) The lubrication process of a bearing under high-speed rotation exhibits a pronounced non-Newtonian fluid feature due to the lubricant's thermal and rheological effects. Therefore, the temperature field and non-Newtonian fluid shearing thinning model are included in the numerical framework.
- (3) Bearings frequently experience insufficient lubrication in actual operating conditions. Thus, the impact of surface roughness topography on oil film thickness must be considered. In this study, we extend the non-Gaussian surface roughness into the mixed TEHL model.
- (4) When compared to dry friction, the stiffness between the ball and the raceway is altered by the presence of a lubricant. The geometric deformations of the contact pair are scrutinized both under dry friction and under lubrication. A modified function correlation between load and elastic deformation under EHL is determined by the derivative definition method, which can enhance the precision of analyzing the mechanical characteristics and lubrication states of bearings.

2. Mathematical Model

2.1. The Quasi-Static Model

A quasi-static model of the angular contact ball bearing is constructed to analyze the mechanical characteristics and motion state. The force analysis and force balance equation solutions for the balls and rings are presented in Jones' work [14]. It is assumed that the outer ring is fixed while the inner ring rotates. The relative coordinate system and contact state between the ball and the inner ring are shown in Figure 1.

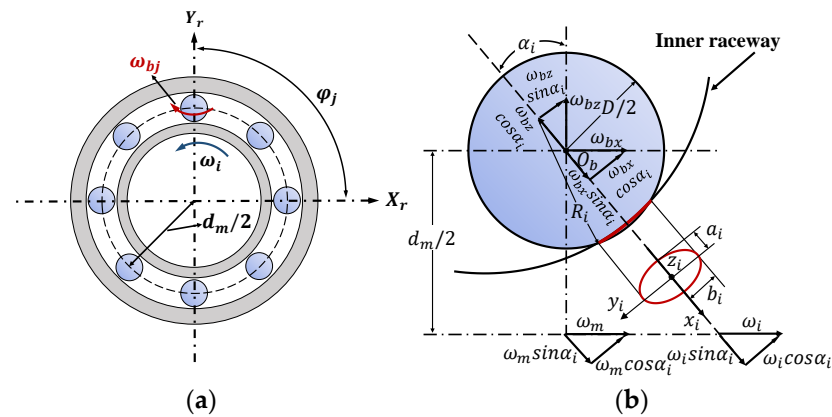


Figure 1. (a) The relative coordinate system of the bearing and (b) contact state of the inner ring.

Nevertheless, a lubricating oil film has an effect on the contact pairs when the lubrication environment is considered. In contrast to dry contact, EHL modifies the pressure distribution and the state of deformation. Figure 2 depicts a comparison of the elastic deformation of the rolling element and the raceway when operating under EHL versus dry contact. According to their geometric structure, they obey the following relationship:

$$h_o = \delta - h_c \tag{1}$$

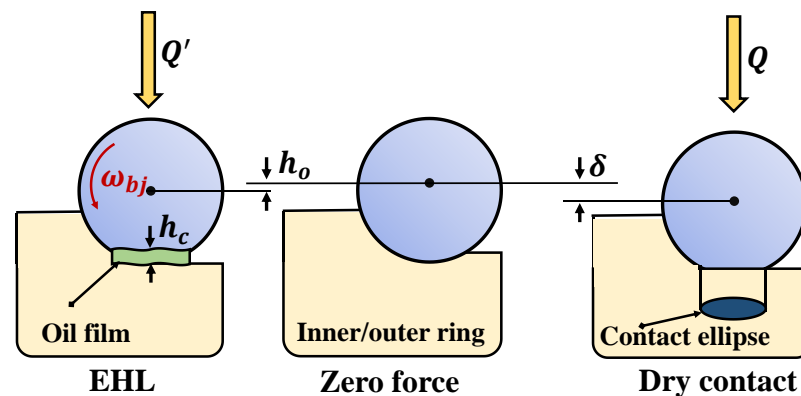


Figure 2. Elastic deformation between the ball and raceway under EHL and dry contact.

As stated in Ref. [14], due to the high rotation speed, the center of the rolling element is not collinear with the center of the groove curvature in the inner and outer rings. Accordingly, the elastic deformation relationship between the inner and outer rings and the ball is shown in Figure 3. While in the EHL, the contact deformation of the inner and outer rings [14] should be modified as follows:

$$\begin{cases} \delta_{ij} = [(A_{1j} - B_{1j})^2 + (A_{2j} - B_{2j})^2]^{1/2} - (f_i - 0.5)D + h_{cij} \\ \delta_{oj} = (B_{1j}^2 + B_{2j}^2)^{1/2} - (f_o - 0.5)D + h_{coj} \end{cases} \tag{2}$$

Identifying the entraining velocities at the contact zone is essential to determine the oil film thickness at the ball–raceway interface. The global/local coordinate system of ball bearings is established, as illustrated in Figure 4. The adjoint coordinate set (O_b, x_b, y_b, z_b) serves as the rolling element’s reference coordinate system.

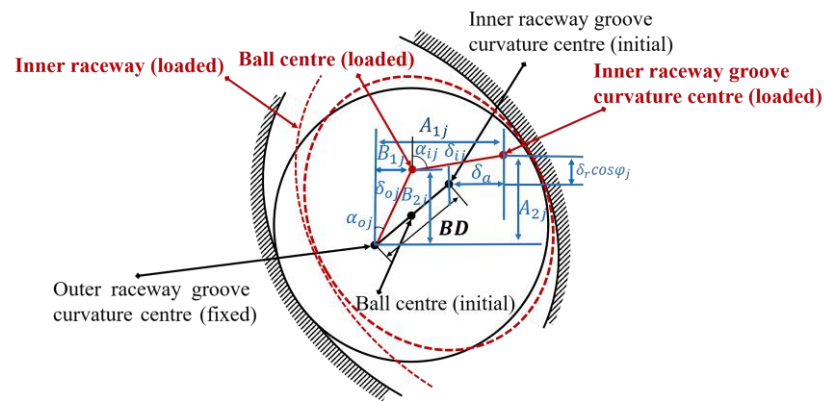


Figure 3. Geometric relationships of the bearing components.

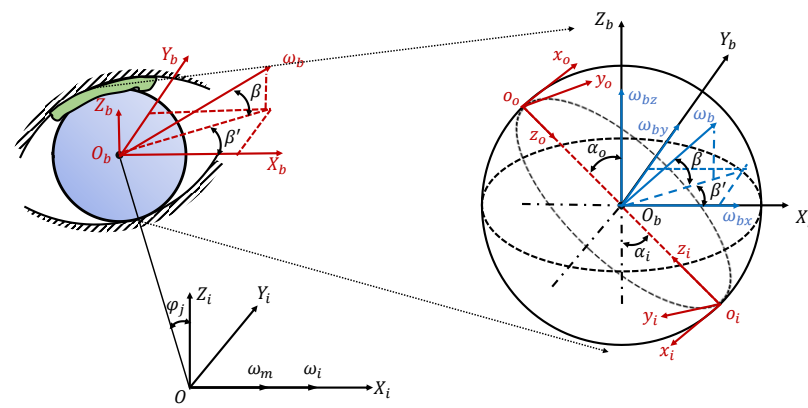


Figure 4. The instantaneous motion geometry diagram of an angular contact bearing.

Taking the balls and inner race conjunctions as an example, as shown in Figures 1b and 4, at the center of the contact region of the inner ring, the linear velocity u_{1i} along the x_i -axis is known to be:

$$u_{1i} = -(\omega_i - \omega_m) \cos \alpha_i (d_m / 2 \cos \alpha_i) - R_i + \sqrt{R_i^2 - a_i^2} - \sqrt{(D/2)^2 - a_i^2} \quad (3)$$

Similarly, the linear velocity u_{2i} along the x_i -axis at the center of the ball's contact zone is:

$$u_{2i} = (\omega_{bx} \cos \alpha_i + \omega_{bz} \sin \alpha_i) \left(R_i - \sqrt{R_i^2 - a_i^2} + \sqrt{(D/2)^2 - a_i^2} \right) \quad (4)$$

Furthermore, the spinning angular velocity of the ball with respect to the inner raceway is:

$$\omega_{si} = (\omega_i - \omega_m) \sin \alpha_i - \omega_b \sin(\alpha_i - \beta) \quad (5)$$

Therefore, the entraining velocity and the slide-roll ratio at the center of the ball-inner raceway contact zone are as follows:

$$\begin{cases} u_{ri} = (u_{1i} + u_{2i}) / 2 \\ S_i = (u_{1i} - u_{2i}) / u_{ri} \end{cases} \quad (6)$$

Hence, the entraining velocities along the x_i and y_i axes for any location in the contact zone are:

$$\begin{cases} u_R(x, y) = u_{ri} - \omega_{si} y_i \\ v_R(x, y) = \omega_{si} x_i / 2 \end{cases} \quad (7)$$

2.2. The Mixed Thermal Elastohydrodynamic Lubrication Model

The Reynolds equation related to the thermal effect and spinning motion of the rolling elements is given by the following form:

$$\frac{\partial}{\partial x} \left[\left(\frac{\rho}{\eta} \right)_e h^3 \frac{\partial p}{\partial x} \right] + \frac{\partial}{\partial y} \left[\left(\frac{\rho}{\eta} \right)_e h^3 \frac{\partial p}{\partial y} \right] = 12 \frac{\partial}{\partial x} (\rho_x u_R h) + 12 \frac{\partial}{\partial y} (\rho_y v_R h) \quad (8)$$

In the formula, $(\rho/\eta)_e = 12(\eta_e \rho'_e/\eta'_e - \rho''_e)$, $\rho_x = [\rho'_e \eta_e (u_2 - u_1) + \rho_e u_1]/u_R$, $\rho_y = [\rho'_e \eta_e (v_2 - v_1) + \rho_e v_1]/v_R$, $\rho_e = (1/h) \int_0^h \rho dz$, $\rho'_e = (1/h^2) \int_0^h \rho \int_0^z (1/\eta) dz' dz$, $\rho''_e = (1/h^3) \int_0^h \rho \int_0^z (z'/\eta) dz' dz$, $1/\eta_e = (1/h) \int_0^h (1/\eta) dz$, $1/\eta'_e = (1/h^2) \int_0^h (z/\eta) dz$.

The equations of film thickness, viscosity, density, load balance, and boundary conditions can be referred to the work of Hu et al. [27]. The energy equation of the lubricant is also introduced to determine the oil temperature distribution as follows:

$$c \left(\rho u \frac{\partial T}{\partial x} + \rho v \frac{\partial T}{\partial y} - q \frac{\partial T}{\partial z} \right) - k \frac{\partial^2 T}{\partial z^2} = - \frac{T}{\rho} \frac{\partial \rho}{\partial T} \left(u \frac{\partial p}{\partial x} + v \frac{\partial p}{\partial y} \right) + \eta \left(\left(\frac{\partial u}{\partial z} \right)^2 + \left(\frac{\partial v}{\partial z} \right)^2 \right) \quad (9)$$

The energy equations for solid rings and balls are:

$$\begin{cases} c_1 \rho_1 \left(u_1 \frac{\partial T}{\partial x} + v_1 \frac{\partial T}{\partial y} \right) = k_1 \frac{\partial^2 T}{\partial z_1^2} \\ c_2 \rho_2 \left(u_2 \frac{\partial T}{\partial x} + v_2 \frac{\partial T}{\partial y} \right) = k_2 \frac{\partial^2 T}{\partial z_2^2} \end{cases} \quad (10)$$

The interface between solids and liquids must satisfy the continuous boundary conditions of heat flow:

$$\begin{cases} k_1 \left(\frac{\partial T}{\partial z_1} \right) \Big|_{z_1=0} = k \frac{\partial T}{\partial z} \Big|_{z=0} \\ k_2 \left(\frac{\partial T}{\partial z_2} \right) \Big|_{z_2=0} = k \frac{\partial T}{\partial z} \Big|_{z=h} \end{cases} \quad (11)$$

The details of the oil film temperature field equations and boundary conditions can be obtained from the work of Guo et al. [28]. The present study employs the Ree–Eyring model to compute the non-Newtonian fluid properties of the lubricants. Liu et al. [29] have provided a description of the constitutive equation of the Ree–Eyring model and the temperature field solution method. Furthermore, in mixed lubrication, the surface roughness amplitude typically commensurate with, or are greater than, the oil film thickness in the contact area. Therefore, it is essential to consider surface roughness and topography in mixed lubrication analysis. A non-Gaussian rough surface was obtained using the digital filter approach for simulation in this paper. The detailed process for generating non-Gaussian rough surfaces can be found in Ref. [30].

3. Numerical Approach

The quasi-static model employed in this study incorporates the mixed TEHL governing equations. The derivative relation of load deformation cannot be obtained by the Hertzian theory. However, as indicated by Equation (1), the central film thickness h_c can be calculated numerically by the mixed TEHL, which has a geometric connection with h_o . Hence, the correlation between the contact load and the contact deformation can be expressed as: $h_o = f_{TEHL}(Q, u, v, T_o, \rho, \eta, \delta, \dots)$. Consequently, applying the derivative definition approach, we can obtain a novel function relation between Q and h_o as follows:

$$\frac{\partial Q}{\partial h_o} = \frac{(Q + \Delta Q) - Q}{h_{o2} - h_{o1}} \quad (12)$$

In this formula, $\Delta Q = 1 \times 10^{-4}$ N was selected as the default value in this paper. The steps for addressing the coupling numerical analysis of the quasi-static bearing model and the mixed TEHL are depicted in Figure 5. Initially, input parameters, such as the structural parameters, material parameters, lubricant properties, and operating conditions are provided for the calculation of a spindle bearing. Next, the quasi-static model is

computed using the Newton–Raphson iteration method to obtain the mechanical features and kinematic states of the bearing. The solution obtained from the numerical calculation of the quasi-static model under dry contact is used as the initial input for the quasi-static model incorporating mixed TEHL to accelerate convergence.

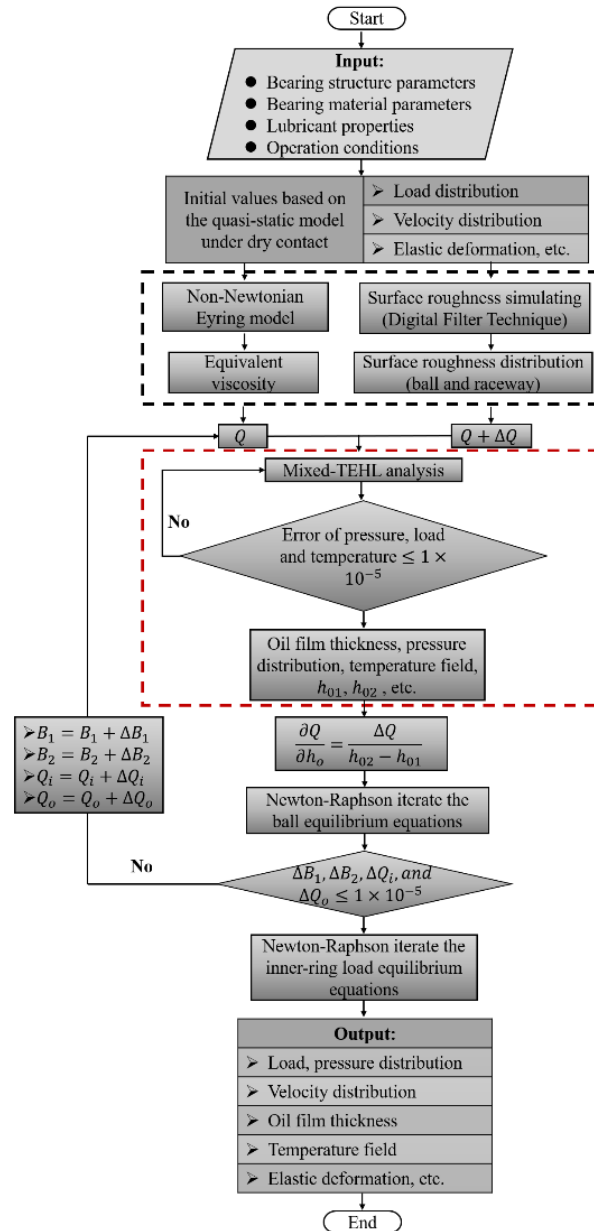


Figure 5. The flow chart of the numerical calculation of the coupling model.

Furthermore, the mixed TEHL model is developed based on the results of the quasi-static model to determine the distribution of the oil film thickness, pressure, and temperature in the contact zone between the balls and the raceways. To overcome the issue of an ill-conditioned coefficient matrix during the discrete process of the Reynolds equation, this study adopted the semi-system method proposed by Ai [31]. In order to expedite the calculation of surface elastic deformation, a DC-FFT technique [32] is incorporated into this study. The temperature field is computed through the column scanning method, and the dimensionless and discrete procedure is in accordance with Ref. [28].

Subsequently, applying the approaching displacement h_o generated by the mixed TEHL, the load equilibrium equations of rolling elements are computed to obtain the updated mechanical properties and kinematic states of the bearing system. The mixed

TEHL algorithm is then iterated to update lubrication performance until convergence is achieved. Once they have converged, the inner raceway load equilibrium is computed. Finally, the load distribution, working contact angle, oil film thickness, temperature field, and other parameters between the rolling elements and raceways are computed. The 7008C angular spindle bearing was selected for this study. Tables 1 and 2 give the material and geometric specifications of the bearing, as well as the physical properties of the lubricating oil. The rotation speed of the inner raceway $n_i = 10,000$ r/min, the axial force $F_a = 500$ N, and ambient temperature $T_o = 303$ K were set as the default operating parameters in the paper.

Table 1. Material and geometry parameters bearing 7008C.

Material Parameters	Value	Geometry Parameters	Value
Elastic modulus of ball/race E_1/E_2 (GPa)	320/207	Ball diameter D (mm)	6.35
Poisson's ratios of ball/race ν_1/ν_2	0.26/0.3	Ball number N	22
Density of ball/race ρ_1/ρ_2 (Kg/m ³)	3120/7850	Initial contact angle (°)	15
Specific heat capacity of ball/race c_1/c_2 (J/Kg·K)	710/460	Inner/outer race curve coefficient f_i/f_o	0.575/0.565
Thermal conductivity of ball/race k_1/k_2 (W/m·K)	30/48	Pitch diameter d_m (mm)	53.32

Table 2. Physical characteristics of the lubricant.

Parameters	Value
Environmental viscosity η_o (Pa·s)	0.033
Environmental viscosity ρ_o (Kg/m ³)	970
Specific heat capacity c (J/Kg·K)	1910
Thermal conductivity k (W/m·K)	0.0966
Viscosity-pressure coefficient (GPa ⁻¹)	18.5
Viscosity-temperature coefficient (K ⁻¹)	0.032
Thermal expansion coefficient	6.5×10^{-4}
Characteristic shear stress τ_o (MPa)	18

4. Results and Discussion

4.1. Model Validation

In order to verify the validity of the proposed algorithm in this paper, the experimental results of Zhang et al. [33] and the theoretical calculation results of Shi et al. [34] were selected as a comparison. The feasibility of this model can be fully proved from the view of experiment and simulation. Since the research objects of Refs. [33,34] are both 476728NQ, this section analyzes the mechanical properties and lubrication performance of this bearing. The related parameters of 476728NQ bearing are listed in Table 3. The parameters of the lubricant in the experiment are given in Table 2. Zhang et al. [33] measured the minimum oil film thickness in the raceway contact zone under various operating conditions by using the resistance capacitance (R-C) oscillation method. Shi et al. [34] analyzed the mechanical properties using a quasi-dynamic model. The experimental conditions used in Refs. [33,34] are given in Table 4.

Table 3. Material and geometry parameters bearing 476728NQ.

Material Parameters	Value	Geometry Parameters	Value
Elastic modulus of ball/race E_1/E_2 (GPa)	218/218	Ball diameter D (mm)	15.4
Poisson's ratios of ball/race ν_1/ν_2	0.3/0.3	Ball number N	18
Density of ball/race ρ_1/ρ_2 (Kg/m ³)	7870/7870	Initial contact angle (°)	26
Specific heat capacity of ball/race c_1/c_2 (J/Kg·K)	460/460	Inner/outer race curve coefficient f_i/f_o	0.515/0.525
Thermal conductivity of ball/race k_1/k_2 (W/m·K)	48/48	Pitch diameter d_m (mm)	182.5

Table 4. Minimum film thickness of experimental conditions by R–C oscillation method.

Operation Condition Number	Axial Load/N	Radial Load/N	Rotation Speed/rpm	Ambient Temperature /°C
#1	15,000	2000	10,000	80
#2	15,000	0	7000	70
#3	15,000	0	10,000	79

In Figure 6, the contact load distributions of bearing rings are analyzed under operating conditions #1 and #3, and the calculation results of the model proposed in this paper are compared with those of the quasi-dynamic model in Ref. [34] and the quasi-static model in Ref. [14]. In the legend, ‘current method’ represents the calculation results of this paper, ‘quasi-static model’ represents the calculation results of Ref. [14], and ‘quasi-dynamic model’ represents the calculation results of Ref. [34]. The findings indicate that the error between the computed results of the current model and those of the quasi-dynamic model is reduced when compared to the quasi-static model. The current model fully incorporates the EHL of the lubricant, thereby compensating for the limitations of the quasi-static model. Furthermore, the current model is constructed with the quasi-static model, which guarantees higher computing efficiency compared to the quasi-dynamic model. Thus, in terms of simulation, the current model may be regarded as an efficient alternative algorithm for the quasi-dynamic model within acceptable error.

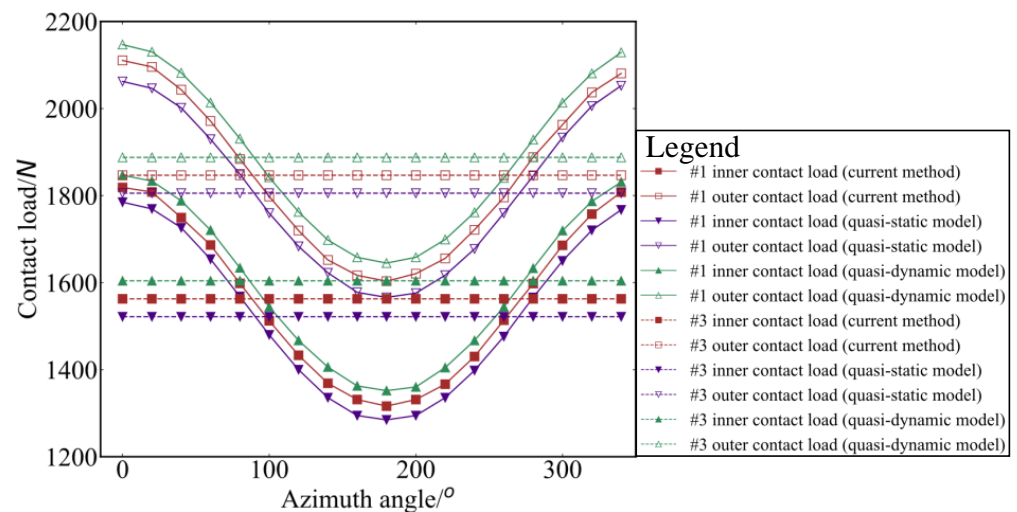
**Figure 6.** Calculation results comparison of bearing rings’ contact load states.

Figure 7 presents a comparison of the minimum oil film thickness achieved through various methods. The focus of examination is the minimum oil film thickness in the inner ring contact zone at an azimuth of 0°. In the legend, ‘‘current method’’ represents the minimum film thickness calculated in this paper, ‘‘H–D’’ represents the minimum film thickness calculated using the fitting formula in Ref. [18], and ‘‘Testing’’ represents the actual minimum film thickness measured by the R–C oscillation experimental method in Ref. [33]. It can be found that the H–D formula has limited applicability due to its inability to account for aspects such as the thermal effect of the lubricant, contact surface roughness, and non-Newtonian fluid characteristics, leading to a significant calculation error. The model developed in this paper takes into account all the aforementioned factors, resulting in theoretical calculations that closely align with the experimental measurements. This further confirms the reliability of the proposed coupling model’s accuracy, as demonstrated through experimental evidence.

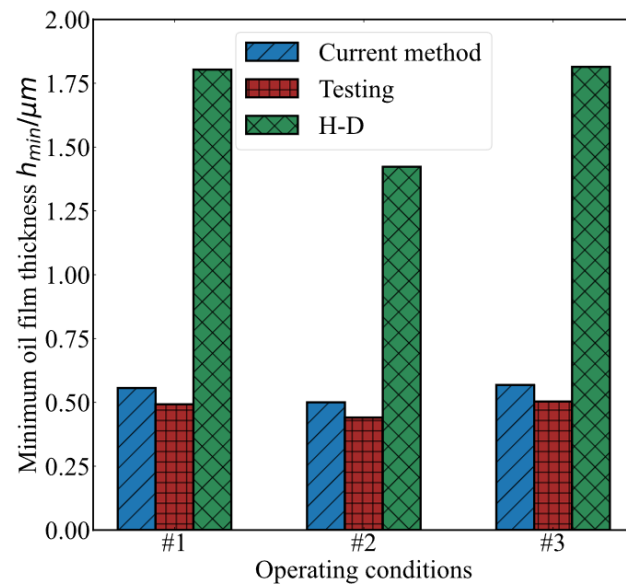


Figure 7. Comparison of the minimum film thickness obtained by various methods.

4.2. Thermal Effects on Mechanical Properties and Lubrication Performance

To investigate the mechanism of the thermal effect, the quasi-static-EHL and quasi-static-TEHL models are solved simultaneously for comparison, both of which ignore the impact of non-Newtonian fluid properties and non-Gaussian surface roughness. Figure 8 depicts a summary of an examination of the heat effect on the lubrication performance in the contact zones between the ball and the raceway under default working conditions. In Figure 8a, we compare the dimensionless oil film thickness and pressure along the x -axis between the ball and the inner ring with and without the thermal effect. Similarly, Figure 8b examines the lubrication states between the ball and the outer ring. The results indicate that the pressure peak in the calculation with the thermal effect is significantly lowered while being blunted and shifted towards the entrance. Furthermore, the oil film distribution has a similar profile under both isothermal and thermal conditions, but the latter experiences a significant decline in thickness due to the decrease in lubricant viscosity, which is induced by the increase in temperature. A decrease in viscosity results in a thinner oil film and poorer lubrication performance.

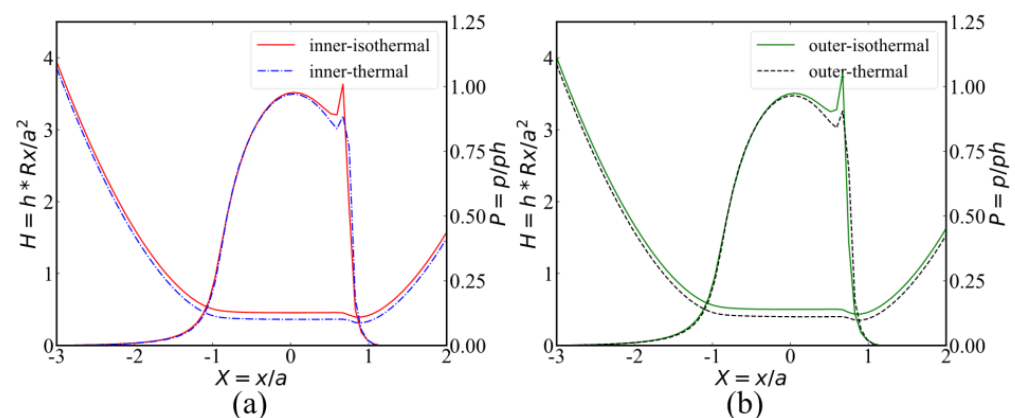


Figure 8. Thermal effects on film thickness and pressure at (a) the inner raceway and (b) the outer raceway.

Figure 9 presents the variations of h_{min} and h_c with respect to rotation speed in the ball–inner ring contact zone. The entraining velocity between the ball and the ring increases with the rotation speed, leading to a rise in both h_{min} and h_c , regardless of whether the thermal effect is considered. Furthermore, it is found that the h_{min} and h_c are thinner under

thermal effect than under isothermal conditions, which is consistent with the variation trend depicted in Figure 8a. This difference becomes more pronounced as the rotation speed goes up.

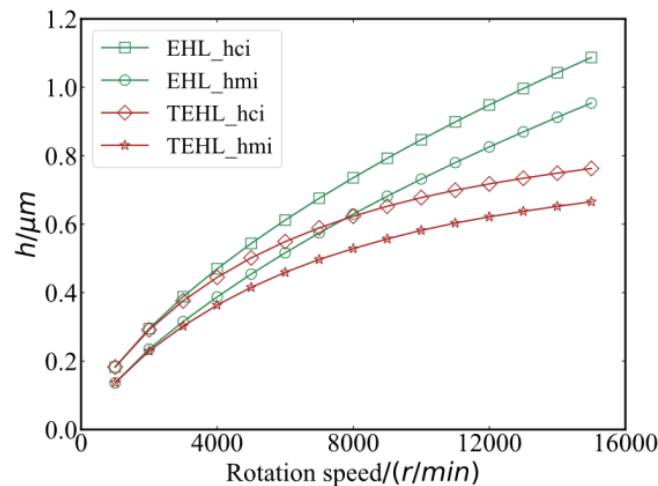


Figure 9. The effect of rotation speed on oil film thickness under different thermal conditions.

Figure 10 shows the thermal effect on the mechanical properties of the bearing. In Figure 10a, three models—quasi-static, quasi-static-EHL, and quasi-static-TEHL—are solved to determine the contact loads between the ball and raceways for comparison. It can be seen that the variation trend of the contact loads with the speed calculated by the three models is completely consistent, which proves that the quasi-static and mixed-TEHL coupling method developed in this work is reasonable. It is noted that as the rotation speed increases, the centrifugal force on the ball increases, causing the outer ring to be compressed and shifting the ball away from the inner ring. Thus, the contact load between the ball and the outer ring (Q_o) gradually rises while the contact load between the ball and the inner ring (Q_i) decreases. Additionally, the quasi-static-EHL and quasi-static-TEHL models give marginally greater results than the quasi-static model due to the presence of lubricating oil film modifying the load deformation relationship of the contact pair. Furthermore, the quasi-static-TEHL predicts a lower contact load than that of the quasi-static-EHL, which can be attributed to the thermal effect weakening the lubrication performance. Figure 10b displays the working contact angles under different inner raceway velocities. It can be seen that the results calculated by the three models evolve consistently with rotation speed. As the speed increases, the working contact angle of the inner ring gradually rises while the working contact angle of the outer ring gradually drops, which is in line with the load evolution trend. Figure 10c shows the axial displacement under different inner race velocities. The results of the quasi-static-EHL and quasi-static-TEHL models are much lower than those of the quasi-static model, and the higher the speed, the more noticeable the deviation. Since elastohydrodynamic lubrication is ineffective at low speed, the result is comparable to that of the quasi-static model. As the speed increases, the effect becomes more prominent, and the contact deformation undergoes significant changes. Figure 10d illustrates the variation of the spinning angular velocity of the inner ring with the inner ring rotation speed, showing that the results of the three models are again reasonably consistent. This suggests that the presence of the lubricating oil film has minimal impact on the spinning angular velocity inside the ball-inner ring contact zone.

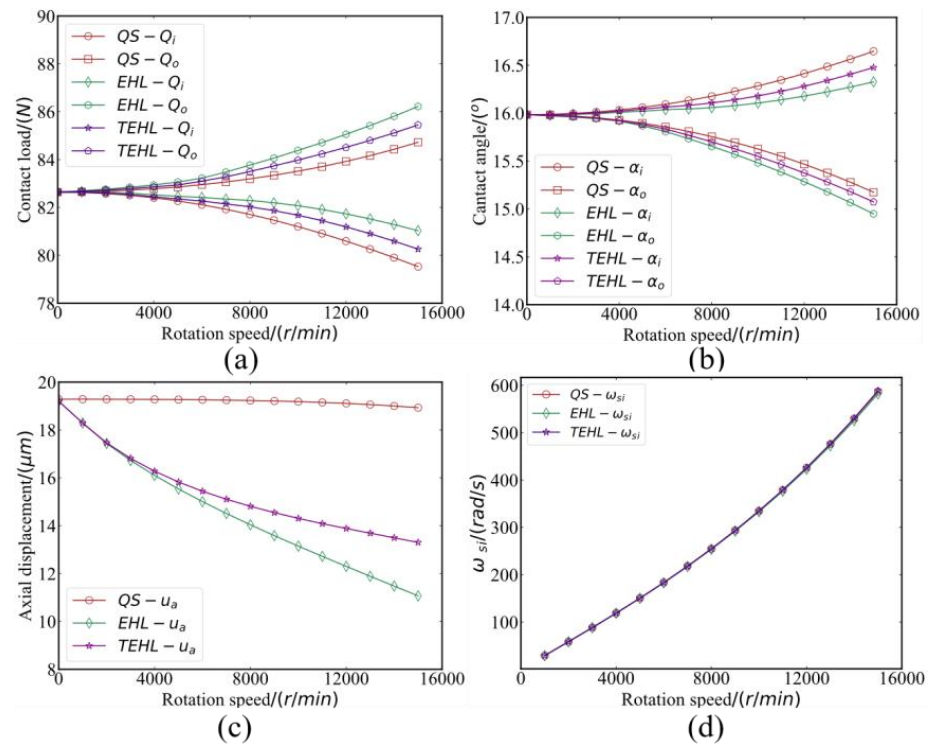


Figure 10. The effects of rotation speed of the inner raceway on (a) contact load; (b) contact angle; (c) axial displacement; and (d) spinning angular velocity.

4.3. Non-Newtonian Effects on Mechanical Properties and Lubrication Performance

For the purpose of analysing the influence of the Ree–Eyring shear thinning model on the mechanical characteristics and lubrication performance of the bearings, this section employs the characteristic shear stress $\tau_0 = 12, 18, 24$ MPa for comparison. The oil film thickness, pressure, and interlayer temperature along the x direction between the ball and the inner ring under various τ_0 are displayed in Figure 11 and are compared to the results of the quasi-static–TEHL model (i.e., the lubricant possesses Newtonian fluid properties). As shown in Figure 11a, the oil film morphology of the non-Newtonian fluid is identical to that of the Newtonian fluid. Hence, the effect of non-Newtonian fluid on oil film thickness can be ignored. According to the inset in Figure 11a, the oil film thickness slightly increases as τ_0 rises. This is because increasing τ_0 enhances the equivalent viscosity of the lubricant, leading to the improvement of the film-forming capabilities. Similarly, the pressure distribution of non-Newtonian fluid is consistent with that of Newtonian fluid, as depicted in Figure 11b. Meanwhile, the phenomenon of the pressure peak moving towards the inlet is also observed, as in Figure 11b.

Figure 12 depicts h_{min} and h_c in the contact zone between the ball and inner ring under various τ_0 and compares them with the results of quasi-static–TEHL. The rotation speed of the inner raceway was changed from 1000 to 15,000 rpm. The variation curves of h_{min} and h_c in the calculation with non-Newtonian fluid almost coincide with the results of Newtonian fluid. As the rotation speed increases to a high level, i.e., over 10,000 rpm, the spinning angular velocity in the inner ring increases sharply, so the thickening rate of the oil film slows down. Furthermore, when the rotation speed is up to 10,000 rpm, both the h_{min} and h_c of non-Newtonian fluid are slightly thinner than those of Newtonian fluid. The film thickness also decreases with the reduction of τ_0 , as seen in the Figure 12.

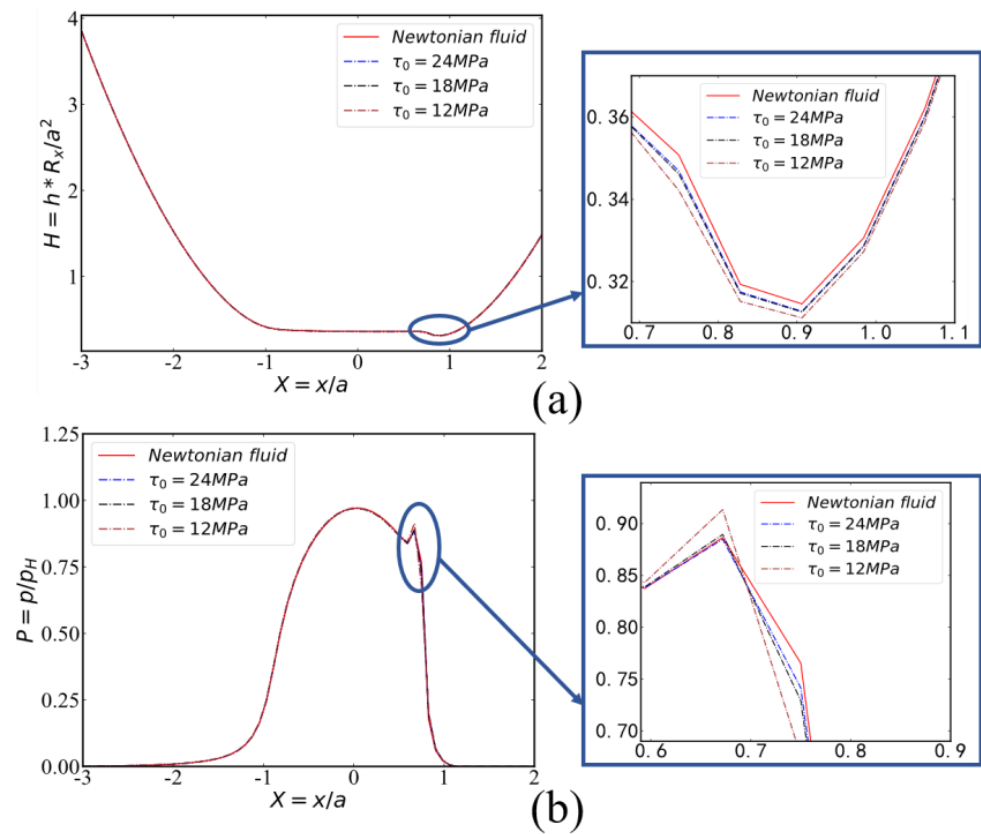


Figure 11. Non-Newtonian fluid effects on (a) film thickness and (b) pressure.

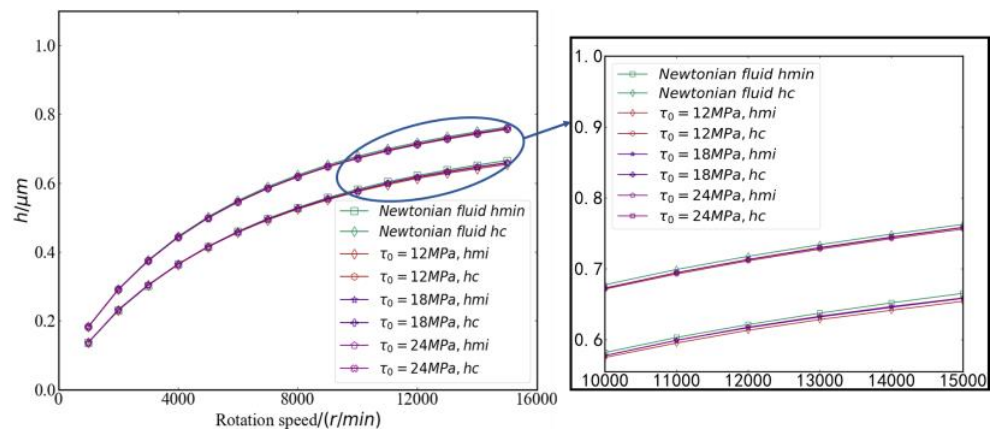


Figure 12. Non-Newtonian fluid effects on oil film thickness under various rotation speed of inner raceway.

In Figure 13, we further examine how non-Newtonian fluids affect bearing mechanical characteristics. In Figure 13a–d, the variation trends of contact load, contact angle, axial displacement, and spinning angular velocity of the inner ring with the inner raceway velocity were investigated and compared with the quasi-static–TEHL model. It is found that the outcomes of non-Newtonian fluid are generally in good agreement with those of Newtonian fluid. Since the lubrication performance of non-Newtonian fluid is identical to that of the Newtonian fluid, hence, the effect of non-Newtonian fluid on the mechanical properties of the bearing can be neglected.

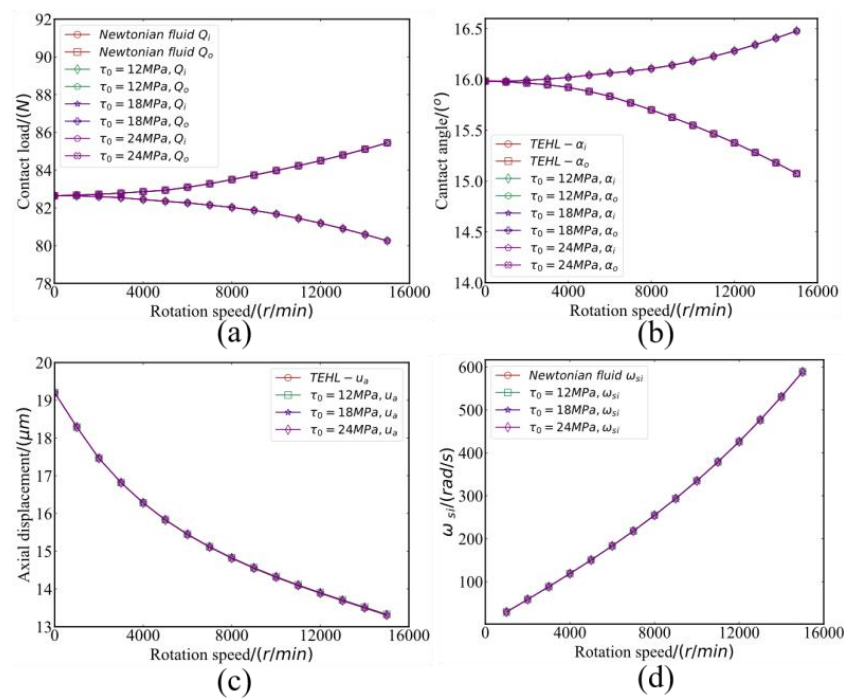


Figure 13. Non-Newtonian fluid effects on (a) contact load; (b) contact angle; (c) axial displacement; and (d) spinning angular velocity.

4.4. Effects of Roughness on Mechanical Properties and Lubrication Performance

4.4.1. Effects of RMS

The ball and raceway have the same roughness parameters as follows: skewness (Ssk) = -1 , kurtosis (Sku) = 8 , $L_x = 10 \mu\text{m}$, $L_y = 50 \mu\text{m}$. h_{min} and h_c are investigated along with the change in RMS and rotation speed, as displayed in Figure 14a. It can be seen that with the increase in RMS, h_{min} decreases while h_c increases. Due to the existence of asperity contact under mixed lubrication, a new evaluation index, average oil film thickness h_a , was introduced to better describe the lubrication and contact performances of the whole zone. The average film thickness is calculated within a certain radius from the center of the normalized Hertzian contact zone, which is set to $2/3$ of the Hertzian contact radius. Since the h_a considers the points within $2/3$ of the Hertzian contact radius, h_a increases with RMS. The increase in RMS results in a deeper roughness valley, so the larger the RMS, the smaller the h_{min} .

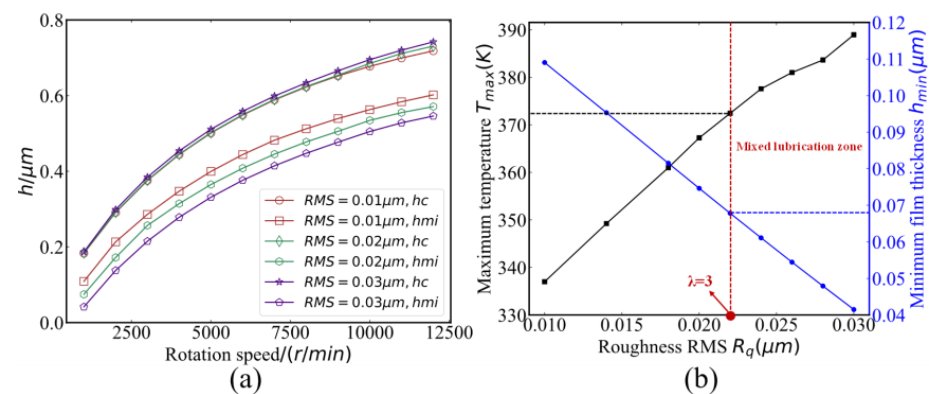


Figure 14. (a) RMS effects on h_{min} and h_c under various rotation speeds and (b) RMS effects on h_{min} and maximum film temperature.

Furthermore, under the harshest working condition, at the rotation speed of 1000 rpm, the influence of RMS on h_{min} and the maximum temperature of the middle oil film layer

are analysed and shown in Figure 14b. These results demonstrate that the oil film thickness falls while the maximum temperature rises with the increase in RMS. It is known that as the friction surfaces become rougher, the flow of lubricant is therefore obstructed, which in turn increases frictional heat generation and decreases film thickness. It should be noticed that the red dotted line in Figure 14b indicates the position of the oil film parameter $\lambda = 3$. This study utilizes the oil film parameter λ ($\lambda = h_{min} / \sqrt{R_{q1}^2 + R_{q2}^2}$) to describe the lubrication states. The critical oil film parameter is $\lambda = 3$, which represents the boundary between full film lubrication and mixed lubrication. The mixed lubrication emerges when $\lambda < 3$, which is attributed to inadequate lubrication and failure. As shown in Figure 14b, when RMS increases to $0.022\mu\text{m}$, $\lambda = 3$, the corresponding minimum film thickness is about $0.066\mu\text{m}$, and the maximum temperature of the interlayer oil film is approximately 372 K.

In Figure 15, the influence of RMS on bearing contact load, contact angle, axial displacement, and inner spinning angular velocity is examined, where ‘smooth’ indicates that contact surface roughness is not considered. Figure 15a demonstrates that as the rotation speed grows, the increase in RMS triggers a modest rise in contact load compared to the smooth surface. With the increase in RMS, the local roughness peak is higher, resulting in a larger h_a , an enhanced elastohydrodynamic effect, and an increased contact load between the friction pairs. Accordingly, in Figure 15b, the contact angle decreases slightly as the RMS increases compared to the smooth surface. Figure 15c demonstrates that as RMS increases, the quantity of axial displacement decreases. However, the RMS has no significant effect on the inner ring’s spinning angular velocity.

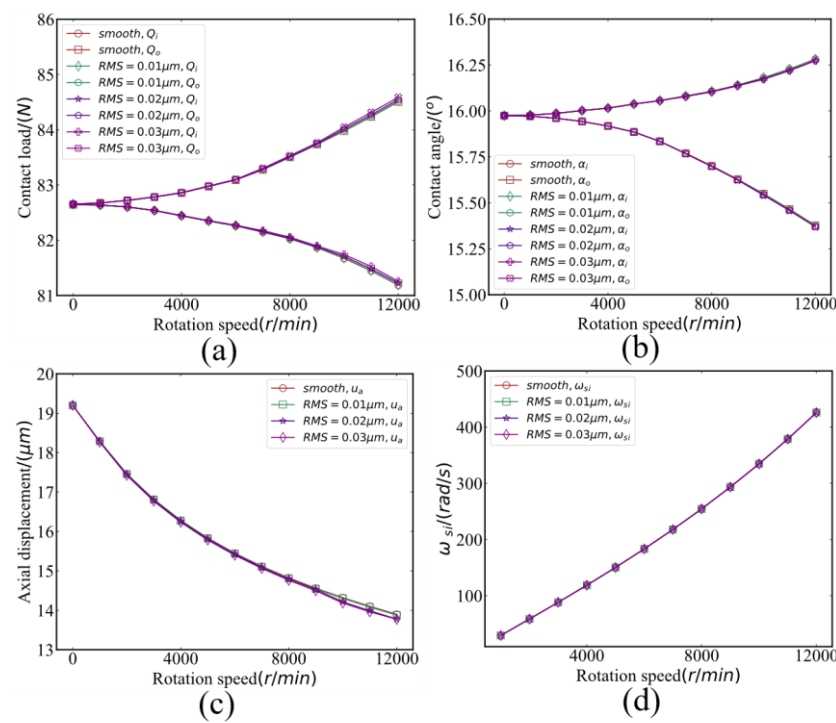


Figure 15. RMS effects on (a) contact load; (b) contact angle; (c) axial displacement; and (d) spinning angular velocity.

4.4.2. Effects of Skewness

This section focuses on the analysis of the effect of surface skewness on the temperature and thickness of oil film. Roughness parameters are selected as follows: $R_q = 0.025\mu\text{m}$, kurtosis (Sku) = 12, $L_x = 20\mu\text{m}$, $L_y = 50\mu\text{m}$. It can be seen from Figure 16a that skewness (Ssk) has less impact on h_c and a more obvious influence on h_{min} . Additionally, under the rotation speed of 1000 rpm, the effects of Ssk on the h_{min} and maximum oil film temperature (T_{max}) of the inner ring and ball contact pair are depicted in Figure 16b. It can be clearly observed that with the increase in Ssk , the h_{min} decreases and the T_{max} increases.

Ssk is usually employed to measure the symmetrical distribution of the roughness peak. When $Ssk > 0$, the surface has more peaks, which is harmful to the formation of the oil film. Hence, surface friction and temperature increase. When Ssk increases to 0.9, $\lambda = 3$, the corresponding minimum film thickness is about $0.075 \mu\text{m}$, and the T_{max} of the interlayer oil film is approximately 387 K.

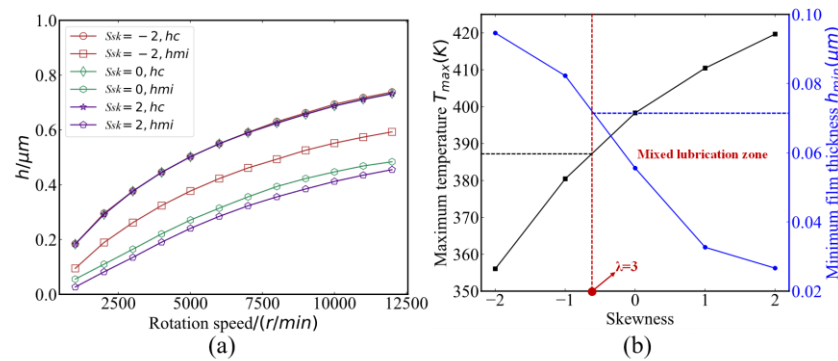


Figure 16. (a) Ssk effects on h_{min} and h_c under various rotation speed and (b) Ssk effects on h_{min} and maximum film temperature.

Furthermore, as depicted in Figure 17, the influence of Ssk on bearing contact load, contact angle, axial displacement, and inner ring spinning angular velocity is negligible.

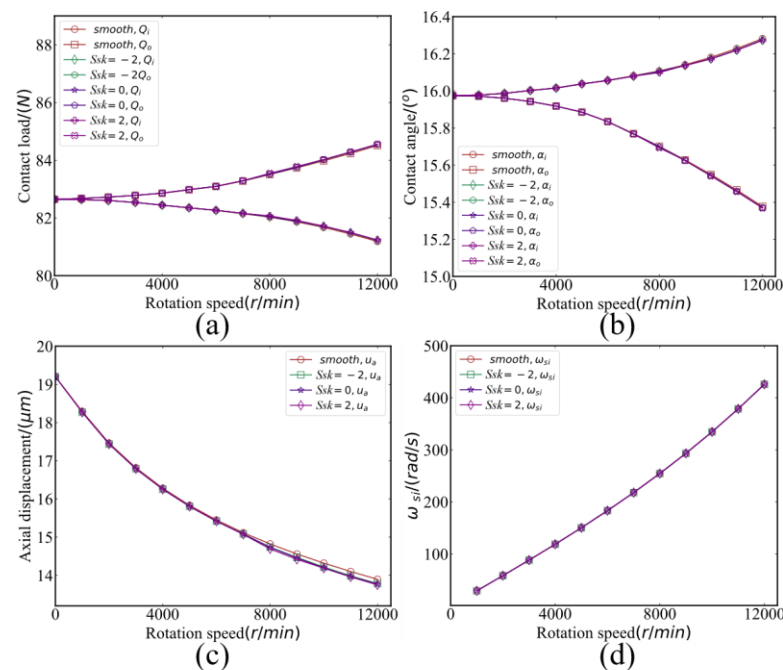


Figure 17. Skewness effects on (a) contact load; (b) contact angle; (c) axial displacement; and (d) spinning angular velocity.

4.4.3. Effects of Kurtosis

In this section, the influence of rough surface kurtosis on bearing lubrication performance is scrutinized. Roughness parameters are selected as follows: $R_q = 0.025 \mu\text{m}$, $Ssk = 1$, $L_x = 20 \mu\text{m}$, $L_y = 50 \mu\text{m}$. It can be seen from Figure 18a that Sku has less impact on h_c and a more obvious influence on h_{min} . Additionally, under the rotation speed of 1000 rpm, the effects of Sku on h_{min} and T_{max} of the inner ring and ball contact pair are presented in Figure 18b. The h_{min} steadily reduces as Sku increases, whereas the T_{max} gradually increases. With the increase in Sku , the probability of surface peak distribution increases, and the local pressure rises, thereby promoting frictional heat generation and

impeding the formation of the lubricating oil film. Additionally, it can be found that when Sk_u increases to 4.5, $\lambda = 3$, the corresponding h_{min} is about $0.075 \mu\text{m}$, and the T_{max} of interlayer oil film is approximately 391 K. Additionally, we investigate the effect of Sk_u on bearing mechanical properties, including contact load, contact angle, axial displacement, and inner ring spinning angular velocity, as described in Figure 19. Similarly, there are no noticeable alterations of Sk_u on the contact angle, axial displacement, or inner ring's spinning angular velocity.

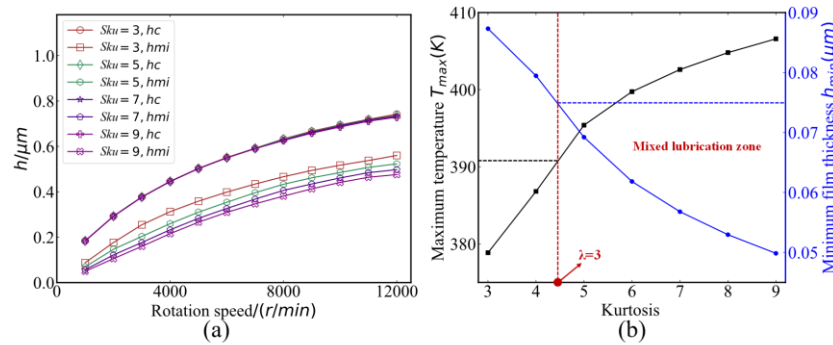


Figure 18. (a) Sk_u effects on h_{min} and h_c under various rotation speeds and (b) Sk_u effects on h_{min} and maximum film temperature.

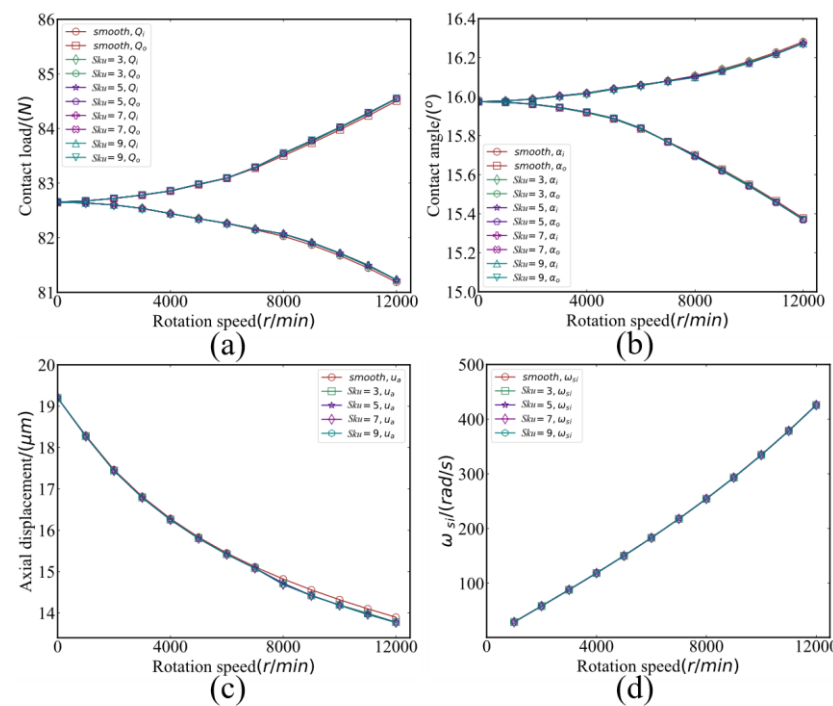


Figure 19. Kurtosis effects on (a) contact load; (b) contact angle; (c) axial displacement; and (d) spinning angular velocity.

4.5. Effects of Operating Parameters on Mechanical Properties and Lubrication Performance

Operating parameters, the externally imposed working conditions of bearings, have a direct impact on the performance of bearings and even affect the structural design and service life. The spindle bearings of high-precision machine tools frequently work under high-speed and low-load conditions. The effect of axial force and rotation speed on the mechanical properties and lubrication performance of the bearing system cannot be overlooked. Therefore, this section will examine the effect of operating parameters on mechanical properties and lubrication performance. The roughness parameters are selected as follows: $R_q = 0.01 \mu\text{m}$, $Ssk = -2$, $Sk_u = 6$, $L_x = 20 \mu\text{m}$, $L_y = 50 \mu\text{m}$.

The h_{min} close to the inner and outer rings of the bearing under various operating conditions are provided in Figure 20. h_{min} of either alongside the inner ring or the outer ring increases with the rotation speed but decreases with the axial load. Under the working conditions of 12,000 r/min and 100 N, h_{min} of the inner and outer rings reach the highest thicknesses, which are 0.65 μm and 0.71 μm , respectively. Overall, the oil film thickness alongside the outer ring is 10% greater than alongside the inner ring. This modest increase is due to the high-speed spinning motion in the inner raceway–ball contact region, severing the working condition. Hence, the lubrication state of the outer ring is better than that of the inner ring. This helps to explain why the spindle bearing of the machine tool often fails preferentially in the inner ring.

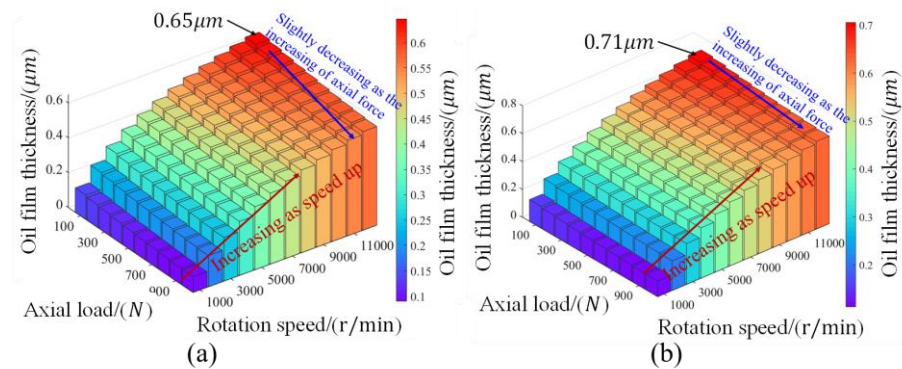


Figure 20. Effects of axial load and rotation speed on h_{min} , alongside (a) the inner ring and (b) the outer ring.

Figure 21 depicts the corresponding T_{max} . It can be obviously seen that as the rotation speed increases, the temperature exhibits a gradual increment. This is because a faster rotation intensifies the frictional heat generation in the contact area, while the higher temperature decreases the viscosity of the lubricant, which therefore weakens the EHL effect. As a consequence, the oil film thickness diminishes, in accordance with the results shown in Figure 20. Additionally, under the working conditions of 12,000 r/min and 1000 N, the T_{max} of the inner and outer rings reach the highest temperatures, which are 469 K and 431 K, respectively, indicating that the inner ring's operating conditions are harsher than those of the outer ring.

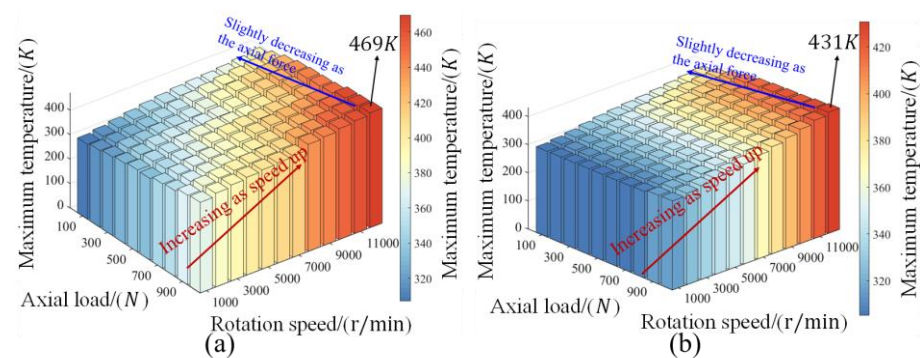


Figure 21. Effects of axial load and rotation speed on T_{max} alongside (a) the inner ring and (b) the outer ring.

According to the results of the foregoing investigation, the operating parameters have a significant impact on the lubrication performance of the bearing system. The mechanical properties will be directly affected by the alterations in the lubrication state. Figure 22 presents the contact load of the inner and outer rings under various operation situations. It can be seen that as the axial load increases, so does the contact load of the inner and outer rings. Figure 22 further indicates that the contact load alongside the inner ring is less than alongside the outer ring.

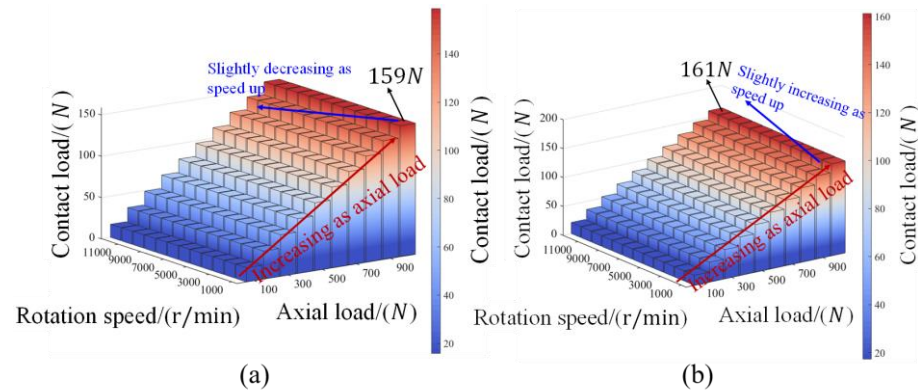


Figure 22. Effects of axial load and rotation speed on contact load alongside (a) the inner ring and (b) the outer ring.

Figure 23 shows the results of the working contact angle. Figure 23a reveals that the working contact angle of the inner ring increases with axial load within 6000 rpm. However, when the speed exceeds 6000 rpm, the working contact angle decreases first and then increases with axial force. In Figure 23b, as the axial load increases, the contact angle of the outer ring also increases. The higher the axial load, the lower the fluctuation of the contact angle. Furthermore, as rotation speed increases, the contact angle of the inner ring increases while the contact angle of the outer ring declines.

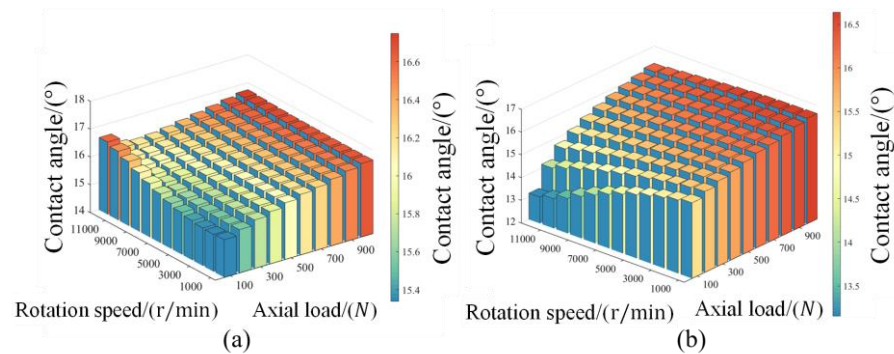


Figure 23. Effects of axial load and rotation speed on contact angle alongside (a) the inner ring and (b) the outer ring.

5. Conclusions

In this paper, a numerical algorithm of quasi-static model coupling with mixed-TEHL is developed to investigate the mechanical properties and lubrication performance of the spindle bearing of high-speed machine tools. The non-Newtonian fluid characteristics, non-Gaussian surface roughness, and the thermal effect are comprehensively examined using the coupled model. The conclusions are as follows:

- (1) Thermal effect decreases the viscosity of the lubricating oil, resulting in a thinner oil film and a reduction in lubrication performance. Therefore, the thermal effect diminishes the EHL effect, leading to a lower contact load and a larger contact angle than the isothermal condition. The oil film temperature between the contact areas of the balls and rings progressively increases as the bearing rotation speed goes up. Under the influence of spinning motion, the y-direction temperature distribution is asymmetrical.
- (2) The calculations of the effect of non-Newtonian lubricant flow on the bearing performance demonstrate that the oil film thickness increases gradually with the increase in τ_0 . Because the equivalent viscosity of the lubricating oil increases with the increase in τ_0 , which improves the oil-film-forming capacity. Furthermore, due to the minor vari-

- ation of oil film thickness under the influence of τ_o , the influence of non-Newtonian fluid characteristics on the mechanical properties of bearings is negligible.
- (3) Examinations of the non-Gaussian parameters on bearing performance indicate that the lubrication state deteriorates as RMS, skewness, and kurtosis increase, i.e., the oil film thickness becomes thinner, and the oil film temperature rises. In addition, as the RMS increases, the bearing contact load increases slightly, the inner ring axial displacement decreases somewhat, and the effect of skewness and kurtosis on the mechanical characteristics of the bearing is negligible.
 - (4) The impact of operating settings on bearing performance is explored. When the rotation speed increases and the axial force decreases, the minimum oil film thickness alongside the inner and outer rings becomes thicker, and the oil film thickness of the outer ring is higher than 10% of the inner ring. With the increase in speed and load, which intensifies the frictional heat generation in the contact area, the oil film temperature gradually rises, while the temperature of the outer ring is lower than that of the inner ring. Furthermore, as the speed increases, the outer ring contact load increases while the inner ring contact load drops. All of the aforementioned information demonstrates that the operating state is the most detrimental factor at the contact area between the ball and the inner ring, where the majority of machine tool spindle bearing incidents occur in practice.

This paper has developed the coupling analysis of quasi-static and thermal mixed-TEHL of machine tool spindle bearings, and investigated the effects of operating conditions, roughness, and non-Newtonian fluid characteristics on the mechanical properties and lubrication performance. However, there are still some issues that need to be further explored in the examination of rolling bearing performance under harsh and complex operating conditions. Furthermore, the severe working environment of bearings is beyond the capabilities of the existing EHL simulation. In the future, large-scale EHL computations will be conducted in the background of big data, so it is critical for the quick collection of tribological performance data for bearing mechanics analysis.

Author Contributions: Conceptualization, Y.C. and H.L.; methodology, H.L.; validation, H.L., Y.C., Y.G., Y.S., D.L. and X.-Q.C.; investigation, H.L. and X.-Q.C.; writing—original draft preparation, H.L.; writing—review and editing, H.L. and Y.C. All authors have read and agreed to the published version of the manuscript.

Funding: This research was funded by the Independent and Controllable Manufacturing of Advanced Bearing (Grant No. XDC04040204).

Data Availability Statement: The data that support the findings of this study are available from the corresponding author upon reasonable request.

Conflicts of Interest: The authors declare that they have no known competing financial interests or personal relationships that could have appeared to influence the work reported in this paper.

Nomenclature

Symbol	Definition	Unit
φ_j	Azimuth of the ball	°
d_m	Pitch diameter of bearing	m
D	Diameter of ball	m
α_i, α_o	Contact angles between the ball and the inner and outer rings	°
a, b	Semimajor and semiminor axes of the contact ellipse	m
ω_i	Angular velocity of the inner ring	rad/s
ω_m	Angular velocity of the ball	rad/s
ω_b	Rotation angular velocity of the ball	rad/s
Q	Normal contact load between the ball and the ring	N
h_o	Approaching displacement between the ball and the ring	m

Symbol	Definition	Unit
h_c, h_{min}	Central oil film thickness and minimum oil film thickness	m
δ_i, δ_o	Elastic deformation of inner ring and outer ring	m
δ_a, δ_r	Axial and radial elastic deformation	m
A_{1j}, A_{2j}	Verical-horizontal distance between inner and outer raceway groove center	m
B_{1j}, B_{2j}	Verical-horizontal distance between ball and outer raceway groove center	m
β, β'	Pitch angle and yaw angle	°
R_i	Hertzian contact radius	m
f_i, f_o	Inner and outer rings' groove curvature coefficient	-
BD	Distance between center of groove curvature of inner ring and outer ring	m
x, y, z	Fixed coordinate system	-
p	Oil film pressure	Pa
h	Oil film thickness	m
η	Dynamic viscosity of the lubricant	Pa·s
ρ, ρ_1, ρ_2	Density of the lubricant, balls and raceways	Kg/m ³
T, T_o	Film temperature and ambient temperature	K
c, c_1, c_2	Specific heat of the lubricant, balls and raceways	J/(Kg·K)
k, k_1, k_2	Thermal conductivity of the lubricant, balls and raceways	W/(m·K)
u, v	Flow velocity along x and y axes	m/s
τ_o	Characteristics shear stress	MPa
RMS/R_q	Root-Mean-Square of roughness	μm
L_x, L_y	Autocorrelation length in x and y axes of roughness	μm
Ssk	Skewness of roughness	-
Sku	Kurtosis of roughness	-

References

- Zhao, J.J.; Lin, M.X.; Song, X.C.; Wei, N. Coupling analysis of the fatigue life and the TEHL contact behavior of ball screw under the multidirectional load. *Ind. Lubr. Tribol.* **2020**, *72*, 1285–1293. [\[CrossRef\]](#)
- Xie, Z.; Wang, Y.; Wu, R.; Yin, J.; Yu, D.; Liu, J.; Cheng, T. A high-speed and long-life triboelectric sensor with charge supplement for monitoring the speed and skidding of rolling bearing. *Nano Energy* **2021**, *92*, 106747. [\[CrossRef\]](#)
- Ardah, S.; Profito, F.J.; Dini, D. An integrated finite volume framework for thermal elasto-hydrodynamic lubrication. *Tribol. Int.* **2023**, *177*, 107935. [\[CrossRef\]](#)
- Kaneta, M.; Matsuda, K.; Wang, J.; Yang, P. Numerical study on effect of dimples on Tribo-characteristics in non-Newtonian thermal elasto-hydrodynamic lubrication point contacts with different mechanical and thermal properties. *J. Tribol.* **2020**, *142*, 041601. [\[CrossRef\]](#)
- Dormois, H.; Fillot, N.; Vergne, P.; Dalmaz, G.; Querry, M.; Ioannides, E.; Morales-Espejel, G.E. First traction results of high spinning large-Size circular EHD contacts from a new test rig: Tribogy. *Tribol. Trans.* **2009**, *52*, 171–179. [\[CrossRef\]](#)
- Doki-Thonon, T.; Fillot, N.; Vergne, P.; Espejel, G.E.M. Numerical insight into heat transfer and power losses in spinning EHD non-Newtonian point contacts. *Proc. Inst. Mech. Eng. Part J J. Eng. Tribol.* **2011**, *226*, 23–35. [\[CrossRef\]](#)
- Pu, W.; Wang, J.; Zhu, D. Friction and flash temperature prediction of mixed lubrication in elliptical contacts with arbitrary velocity vector. *Tribol. Int.* **2016**, *99*, 38–46. [\[CrossRef\]](#)
- Yan, X.-L.; Wang, X.-L.; Zhang, Y.-Y. A numerical study of fatigue life in non-Newtonian thermal EHL rolling–sliding contacts with spinning. *Tribol. Int.* **2014**, *80*, 156–165. [\[CrossRef\]](#)
- Yan, X.; Zhang, Y.; Xie, G.; Qin, F.; Zhang, X. Effects of spinning on the mixed thermal elasto-hydrodynamic lubrication and fatigue life in point contacts. *Proc. Inst. Mech. Eng. Part J J. Eng. Tribol.* **2019**, *233*, 1820–1832. [\[CrossRef\]](#)
- Doki-Thonon, T.; Fillot, N.; Espejel, G.E.M.; Querry, M.; Philippon, D.; Devaux, N.; Vergne, P. A dual experimental/numerical approach for film thickness analysis in TEHL spinning skewing circular contacts. *Tribol. Lett.* **2013**, *50*, 115–126. [\[CrossRef\]](#)
- Amine, G.; Fillot, N.; Philippon, D.; Devaux, N.; Dufils, J.; Macron, E. Dual experimental-numerical study of oil film thickness and friction in a wide elliptical TEHL contact: From pure rolling to opposite sliding. *Tribol. Int.* **2023**, *184*, 108466. [\[CrossRef\]](#)
- Nonato, F.; Cavalca, K.L. An approach for including the stiffness and damping of elasto-hydrodynamic point contacts in deep groove ball bearing equilibrium models. *J. Sound Vib.* **2014**, *333*, 6960–6978. [\[CrossRef\]](#)
- Questa, H.; Mohammadpour, M.; Theodossiades, S.; Garner, C.; Bewsher, S.; Offner, G. Tribo-dynamic analysis of high-speed roller bearings for electrified vehicle powertrains. *Tribol. Int.* **2020**, *154*, 106675. [\[CrossRef\]](#)
- Jones, A.B. A General theory for elastically constrained ball and radial roller bearings under arbitrary load and speed conditions. *J. Basic Eng.* **1960**, *82*, 309–320. [\[CrossRef\]](#)

15. Shi, X.-J.; Wang, L.-Q.; Mao, Y.-Z.; Qin, F.-Q. Coupling study on dynamics and TEHL behavior of high-speed and heavy-load angular contact ball bearing with spinning. *Tribol. Int.* **2015**, *88*, 76–84. [[CrossRef](#)]
16. Li, Y.L.; Wang, W.Z.; Zhao, Z.Q.; Kong, L.J. Calculation on EHL temperature field based on moving point heat source integration method. *Lubr. Eng.* **2014**, *39*, 43–47.
17. Bal, H.; Aktürk, N. Vibration modeling of wind turbine shaft as rigid shaft supported by EHL contact ball bearings with overhung disc system. *Tribol. Int.* **2020**, *151*, 106481. [[CrossRef](#)]
18. Hamrock, B.J.; Dowson, D. Isothermal elastohydrodynamic lubrication of point contacts: Part 1—Theoretical Formulation. *J. Lubr. Technol.* **1976**, *98*, 223–228. [[CrossRef](#)]
19. Sun, H.Y.; Zhang, Y.P.; Guan, D.Z.; Zhang, P.G. Study on the suitability for the Hamrock-Dowson formula under heavy load and high-speed working conditions. *J. Qingdao Univ. Eng. Technol. Ed.* **2011**, *26*, 82–85.
20. Guo, K.; Yuan, S.H.; Zhang, Y.Y.; Wang, X.L. Study on the calculation method of ball bearing mechanical characteristics considering elastohydrodynamic lubrication with spinning. *J. Mech. Eng.* **2013**, *49*, 62–67. [[CrossRef](#)]
21. Tian, J.; Zhang, C.; Liang, H.; Guo, D. Simulation of the load reduction process of high-speed angular contact ball bearing with coupling model of dynamics and thermo-elastohydrodynamic lubrication. *Tribol. Int.* **2021**, *165*, 107292. [[CrossRef](#)]
22. Wu, J.; Wang, L.; He, T.; Gu, L.; Zhang, C.; Lu, Y. Investigation on the angular contact ball bearings under low speed and heavy load with coupled mixed lubrication and quasi-dynamic analysis. *Lubr. Sci.* **2020**, *32*, 108–120. [[CrossRef](#)]
23. Gao, S.; Chatterton, S.; Pennacchi, P.; Han, Q.; Chu, F. Skidding and cage whirling of angular contact ball bearings: Kinematic-hertzian contact-thermal-elasto-hydrodynamic model with thermal expansion and experimental validation. *Mech. Syst. Signal Process.* **2021**, *166*, 108427. [[CrossRef](#)]
24. Shuai, Q.Q.; Chen, X.Y.; Chen, S.J.; Zhang, Y. Influences of preload methods on internal mechanical characteristics of angular contact ball bearings under elastohydrodynamic lubrication. *Tribology* **2022**, *42*, 85–94.
25. Peta, K.; Bartkowiak, T.; Rybicki, M.; Galek, P.; Mendak, M.; Wiczorowski, M.; Brown, C.A. Scale-dependent wetting behavior of bioinspired lubricants on electrical discharge machined Ti6Al4V surfaces. *Tribol. Int.* **2024**, *194*, 109562. [[CrossRef](#)]
26. Zmarzły, P. Influence of bearing raceway surface topography on the level of generated vibration as an example of operational heredity. *Indian J. Eng. Mater. Sci.* **2020**, *27*, 356–364. [[CrossRef](#)]
27. Hu, Y.-Z.; Zhu, D. A Full Numerical Solution to the Mixed Lubrication in Point Contacts. *J. Tribol.* **1999**, *122*, 1–9. [[CrossRef](#)]
28. Guo, F.; Yang, P.; Qu, S. On the theory of thermal elastohydrodynamic lubrication at high slide-roll ratios—Circular glass-steel contact solution at opposite sliding. *J. Tribol.* **2000**, *123*, 816–821. [[CrossRef](#)]
29. Liu, X.; Jiang, M.; Yang, P.; Kaneta, M. Non-Newtonian thermal analyses of point EHL contacts using the Eyring model. *J. Tribol.* **2005**, *127*, 70–81. [[CrossRef](#)]
30. Hu, Y.; Tonder, K. Simulation of 3-D random rough surface by 2-D digital filter and fourier analysis. *Int. J. Mach. Tools Manuf.* **1992**, *32*, 83–90. [[CrossRef](#)]
31. Ai, X.; Cheng, H.S.; Zheng, L. A transient model for micro-elastohydrodynamic lubrication with three-dimensional irregularities. *J. Tribol.* **1993**, *115*, 102–110. [[CrossRef](#)]
32. Liu, S.B.; Wang, Q.; Liu, G. A versatile method of discrete convolution and FFT (DC-FFT) for contact analysis. *Wear* **2000**, *243*, 101–111. [[CrossRef](#)]
33. Zhang, P.S.; Zhai, W.J.; Zhan, M.X.; Shao, J.X.; Wang, H.Q.; Xiao, B.Q. Test study on elastohydrodynamic oil film state of three typical mainshaft bearings of aero-engine. *Synth. Lubr.* **1994**, *1*, 1–4.
34. Shi, X.J.; Wang, L.Q.; Gu, L.; Zheng, D.Z.; Zhao, X.L. Thermal elastohydrodynamic lubrication analysis of aero-engine mainshaft ball bearing based on quasi-dynamic. *J. Aerosp. Power* **2016**, *31*, 233–240.

Disclaimer/Publisher’s Note: The statements, opinions and data contained in all publications are solely those of the individual author(s) and contributor(s) and not of MDPI and/or the editor(s). MDPI and/or the editor(s) disclaim responsibility for any injury to people or property resulting from any ideas, methods, instructions or products referred to in the content.